CYCLIC BEHAVIOR OF RC SUBASSEMBLAGES UPGRADED WITH COMPOSITES

Andrea Prota, University of Naples Federico II, Naples, ITALY
Gaetano Manfredi, University of Naples Federico II, Naples, ITALY
Antonio Nanni, University of Missouri-Rolla, Rolla, MO, USA
Edoardo Cosenza, University of Naples Federico II, Naples, ITALY

Introduction

The seismic strengthening of existing RC structures represents an important issue in many areas of the world. Such a problem becomes of particular relevance in the case of gravity load designed (GLD) frames, built without seismic provisions; they are then characterized by an unsatisfactory structural behavior due to the low available ductility and the lack of a strength hierarchy inducing global failure mechanisms. The seismic upgrade of GLD structures is aimed at strengthening its members allowing more strength and/or ductility and energy dissipation. The final objective could be obtained by a local upgrade of members in order to achieve a ductile global behavior. The lower bound in the strength hierarchy of the frame performance pertains to column failure and it could represent a typical condition of GLD structures. The upgrade of columns by providing them with a higher confinement level and/or with more flexural reinforcement could cause the failure to occur in the nodal zone (i.e., shear failure of the joint, intermediate level of the strength hierarchy); the joint should be also strengthened in order to move up along the strength hierarchy toward its upper bound (i.e., formation of plastic hinges in the beams). Along with boosting the strength and the ductility, the seismic upgrade should also increase the energy dissipation capacity of the structure. A criterion used for assessing the seismic behavior of RC structures is based on comparing the amount of energy that can be dissipated with a limit value (Uang and Bertero 1990). In this way, the energy demand generated by a seismic event (Manfredi 2001) is compared to the energy that the structure is able to supply. Therefore, within a supply-demand approach, it is very important to evaluate how different FRP strengthening solutions can influence the dissipation capacity. The outcomes of such analysis need to be merged with those related to the key parameters of a performance-based design (story drift and stiffness).

An experimental program on interior RC beam-column connections was performed at the University of Missouri-Rolla (Missouri, USA) in order to validate an innovative solution for the seismic upgrade of interior RC subassemblages. The proposed technique is based on the combined use of FRP laminates and near surface mounted (NSM) bars; the laminates are installed by manual lay-up and impregnated in-situ, while FRP NSM bars are applied in epoxy filled grooves. It was demonstrated that such a technique could allow for a selective upgrade of RC connections by choosing different combinations and location of laminates and bars. The main parameters investigated within the experimental campaign were: the axial load ratio of the column, P, the type of FRP reinforcement (laminates and/or NSM bars), and the amount of applied FRP composites. Details on conducted tests were provided in Prota et al. (2002a). In the following discussion, specimens are denoted with a code showing a letter and a number. Letters L and H are used in order to distinguish specimens with axial load ratio on the superior column equal to 0.1 and 0.2, respectively. Control connections are indicated with number 1. Subassemblages with wrapped columns are denoted with 2, while the number 3 is assigned to specimens whose columns were

strengthened with both FRP NSM bars and wrapping. The number 4 is finally adopted for those connections where the joint was strengthened along with columns.

Capacity of Subassemblage Components

Columns and Beams

The strength assessment of the subassemblage requires taking into account the hierarchy between different members. By separately computing the capacity of columns, beams and joint, the strength of the sub-system can be evaluated as that provided by its weakest component. For both columns and beams, a sectional analysis was carried out in Prota et al. (2002b): Table 1 summarizes the results. For each subassemblage, both superior and inferior columns were considered in order to account for the different axial load, P, due to gravity loads on the beams. The shear values in the column at yielding of longitudinal column steel bars, T^C_{yc}, and at failure of the column, T^C_{uc}, were computed. The columns were analyzed by dividing the cross-section into strips and deriving lateral strains based on the axial strains due to combined axial load and bending. Three different constitutive relationships were used for concrete, namely: unconfined, confined only with FRP, and confined with combined externally bonded laminates and internal steel hoops (Realfonzo et al. 2002). For the beams, two cross-section configurations (before and after shear inversion) needed to be considered in order to account for the inversion of the shear force resulting in an opposite moment sign on the element (Prota et al. 2002a). The shear forces in the column at yielding of beam steel bars, T^C_{yb}, and at failure of the beam, T^C_{ub}, were then calculated for both cross-section configurations.

Joint

The stress analysis within the joint was carried out following the Paulay and Priestley approach (1992). The analysis focused on two main stages: first cracking and shear crisis of the joint (Prota et al. 2002b). Seismic guidelines (such as ATC40 1996) consider cracking initiation in the joint as a first level of degradation of the frame: this was the reason for considering stage along with ultimate conditions. The last column of Table 1 reports experimental values of column shear at first cracking of the joint, T^C_{crj}. Since the joint region was not instrumented during tests, cracking initiation was detected based on the appearance of first diagonal cracks in the nodal zone. Such visual methodology could not be applied in the case of connections H4 and L4 where the joint was covered with FRP laminates; that is why column shear values at first cracking of these connections do not appear in Table 1.

Within a performance-based approach (Ghobarah 2001), the story drift angle is a reference parameter in order to evaluate the ductility of RC frames (FEMA 356); Priestley (1997) showed that the deficiencies of their seismic performance are mainly related to the lack of ductility. Since the tested subassemblage represents an extracted portion of the frame, its story drift angles are representative of the actual behavior of the real structure. On the other hand, a stiffness assessment could allow evaluating the dynamic properties of RC frames. The analysis of story drift angle and stiffness for tested subassemblages is carried out in following sections. Since repetitions were performed for each load level, drift and stiffness corresponding to the first load application per cycle were considered. The descendent branch of each curve was stopped at a column shear equal to about 95% of the ultimate.

Table 1. Theoretical Column Shear at Yielding and Failure for Both Column and Beam and Experimental Column Shear at First Cracking of the Joint

Specimen	Column	P (kN)	T^C_{yc} (kN)	T^C_{uc} (kN)	Beam	T^C_{yb} (kN)	T^C_{ub} (kN)	T^C_{crj} (kN)
L1	superior	124.5	31.6	32.7	before	99.3	104.0	15.8
	inferior	204.6	36.3	37.3	after	115.3	128.7	
L2	superior	124.5	31.7	33.7	before	99.9	104.2	15.8
	inferior	204.6	36.3	37.5	after	115.5	128.7	
L3	superior	124.5	46.5	92.5	before	99.3	104.0	26.3
	inferior	204.6	51.1	93.5	after	115.3	128.7	
L4	superior	124.5	46.3	91.5	before	99.2	103.5	------
	inferior	204.6	50.7	92.7	after	115.3	128.6	
H1	superior	249.0	37.7	38.3	before	98.0	102.3	15.8
	inferior	329.0	41.3	42.0	after	115.1	128.6	
H2	superior	249.0	38.4	39.2	before	99.2	103.5	21.0
	inferior	329.0	42.4	43.1	after	115.3	128.6	
H3	superior	249.0	52.0	90.0	before	98.0	102.3	21.0
	inferior	329.0	55.6	90.8	after	115.1	128.6	
H4	superior	249.0	53.5	93.9	before	99.9	104.2	------
	inferior	329.0	57.4	95.0	after	115.5	128.7	

Story Drift Angle and Stiffness of the Subassemblage

Story Drift Angle

Figures 1 and 2 show the behavior of tested subassemblages in terms of column shear versus story drift angle. The fuse defined by all curves is generally narrower for series L than for H, showing lower drift differences for specimens belonging to the same series and characterized by different upgrade schemes. Generally, for the same column shear, type L connections provide larger drift angles than type H: this is due to the influence of the axial load that reduces the deformability of the system. Table 2 summarizes story drift angles corresponding to the maximum column shear, δ_{max}, and to the 95% of the maximum column shear on the descendent branch, $\delta_{95\%}$. For type H connections, the column wrapping allows for more ultimate ductility (i.e., 3.50 vs. 2.82) and such difference becomes even higher at 5% of strength deterioration (i.e., 6.05 vs. 3.80). This is not true if the column is strengthened with both NSM bars and laminates: at ultimate, the story drift provided by H3 is lower than H1 (i.e., 2.42 vs. 2.82), while at 95% of the ultimate strength the ductility of H3 becomes higher than H1 (i.e., 3.80 vs. 3.21). The strengthening of the joint (H4) determines indeed an increased ductility either at ultimate (i.e., 4.27 vs. 2.82) or at 95% of the ultimate (i.e., 4.80 vs. 3.21). Within series L, connection L2 shows lower ductility than L1 at ultimate (i.e., 2.76 vs. 3.11), while its story drift angle is higher than L1 at 95% of the maximum strength (i.e., 3.25 vs. 3.13). Further strengthening of column (i.e., L3) and of joint (i.e., L4) causes story drift angles higher than those of the control specimen both at ultimate (i.e., 3.30 and 5.38 vs. 3.11) and at 95% of the ultimate resistance (i.e., 4.05 and 5.52 vs. 3.13). It is important to underline that different concrete strengths of tested subassemblages affect the results as reported (Prota et al. 2002a). Table 2 shows that wrapping of columns makes descendent branches less brittle, with story drift angles at 95% of the ultimate much higher than control specimens. This represents an additional resource that the structural system can provide during the response under seismic actions. On the other hand, specimens L4 and H4 show a very brittle descendent branch; this is due to the failure mechanism (crisis at column-joint interface) and to the fact that the FRP strengthening of the joint reduces deformability.

Table 2. Story Drift Angle at Ultimate and at 95% of Ultimate

Specimen	δ_{max} (%)	$\delta_{95\%}$ (%)	$\delta_{95\%}$ /δ_{ult}
L1	3.11	3.13	1.01
L2	2.76	3.25	1.18
L3	3.30	4.05	1.23
L4	5.38	5.52	1.03
H1	2.82	3.21	1.14
H2	3.50	6.05	1.73
H3	2.42	3.80	1.57
H4	4.27	4.80	1.12

Cyclic Stiffness

The stiffness was computed on column shear-drift angle curves depicted in Figures 1 and 2. As the sketch of Figure 3 shows, the secant stiffness (Higazy and Elnashai 1997) was calculated at maximum column shear corresponding to the first application of each level of seismic load. Due to the adopted setup, the load was applied cyclically only up to a certain level; then the specimen was taken to failure with a monotonic load (Prota et al. 2002a). The secant stiffness was computed on the first cycle in case of repetitions (Figure 3) and, finally, from points of the monotonic curve.

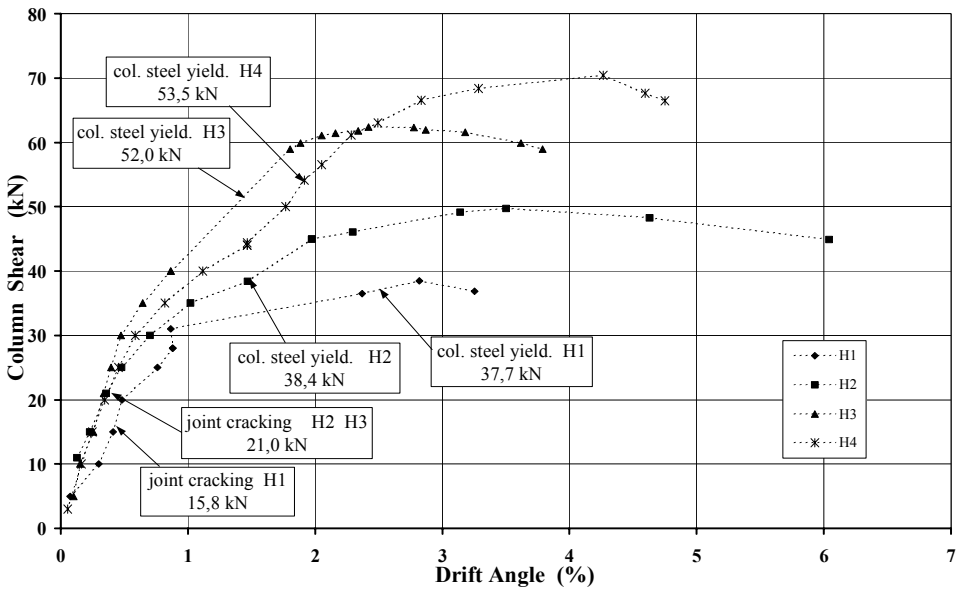

Figure 1. Column Shear vs. Story Drift Angle after the First Load Repetition: H Connections

Stiffness trends for each series of specimens are depicted in Figures 4 and 5. Again, the fuse defined by series L is narrower than that for series H, indicating less scatter in stiffness due to different upgrade schemes. As the comparison performed for column shears of 25 , 30 , 35 and 40 kN, confirms (Figure 6), connections subjected to low axial load ratio (i.e., series L) are generally less stiff than type H. While such difference is not that high for control and only wrapped specimens (i.e., 1 and 2), a significant gap characterizes connections with major upgrade level. Within each series, control specimens (i.e., H1 and L1) show the lowest stiffness up to failure (Figures 4 and 5).

For other upgrade schemes, the following remarks can be underlined. After cracking of joint H2 and H3 (column shear of 21 kN), connection H3 becomes clearly stiffer than H4, whose curve is intermediate between H2 and H3. In the case of series L, between first cracking of L2 (column shear of 15.8 kN) and L3 (column shear of 26.3 kN), L2 is the stiffest, while L3 is intermediate between L2 and L4. Joint cracking of L3 and then steel yielding of L2 (column shear of 31.6) change the trend and the three subassemblages give very similar stiffness values. Shear values reported in Figures 4 and 5 allow observing how the trend of each curve is influenced by the occurrence of joint cracking or steel yielding.

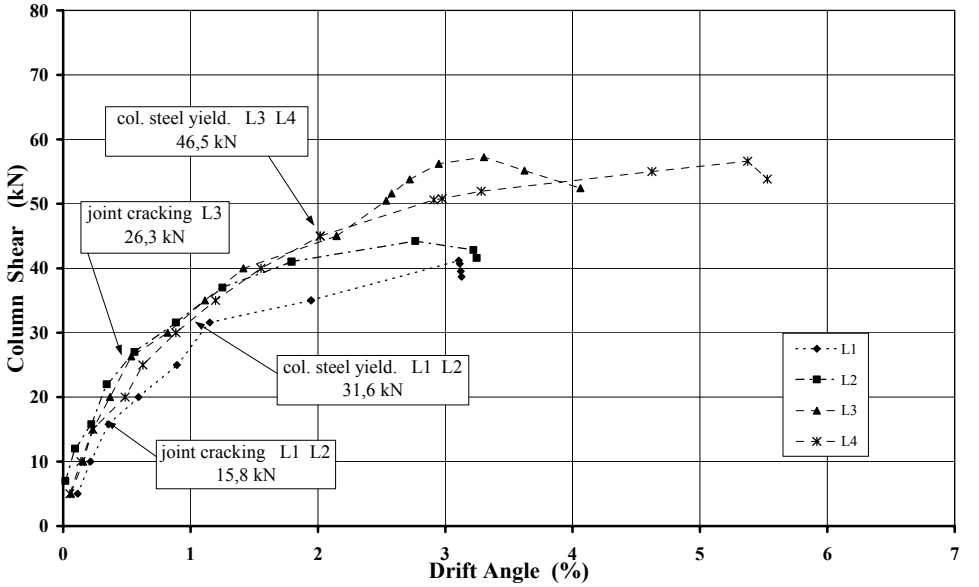

Figure 2. Column Shear vs. Story Drift Angle after the First Load Repetition: L Connections

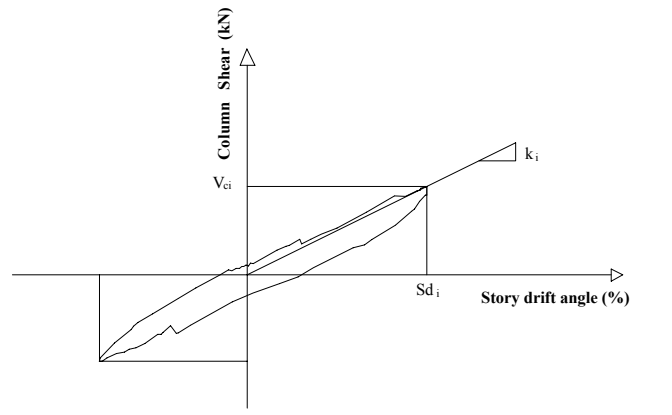

Figure 3. Secant Stiffness

Total Energy

The dissipated energy was computed as the area inscribed by the hysteresis loops of the column shear versus story drift angle, as depicted in Figure 10-a (Higazy and Elnashai 1997). Figures 7 and 8 show the column shear versus the total energy. Since three load repetitions were

performed for each load level "i", three energy values correspond to the same column shear. In Figures 7 and 8, the total energy at each step was obtained by adding the sum of previous energies to the energy given by the last loop. In the following sections, remarks on total energy values are proposed first for each series (i.e., H and L) and then for specimens with the same upgrade scheme.

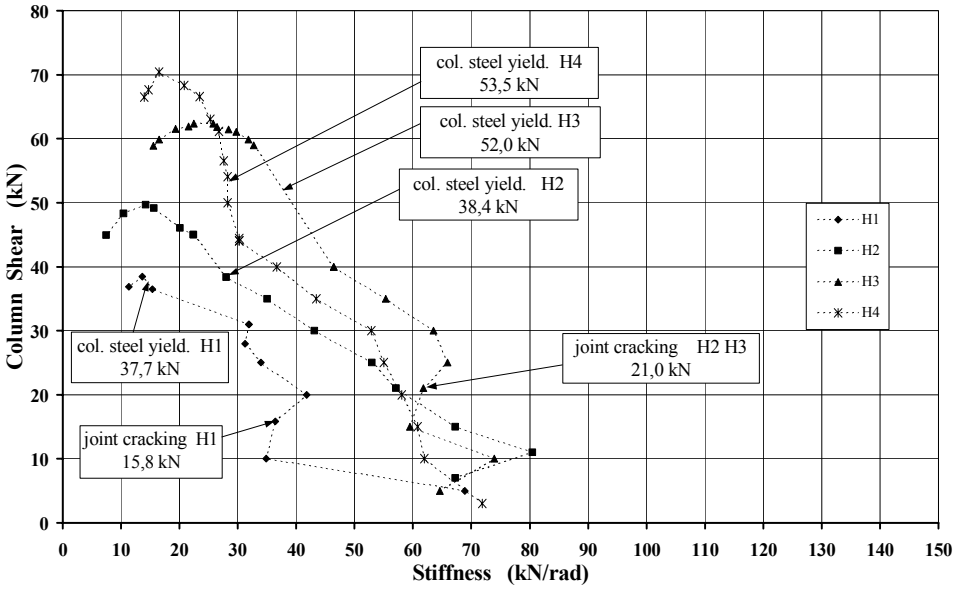

Figure 4. Column Shear vs. Secant Stiffness for Type H Connections

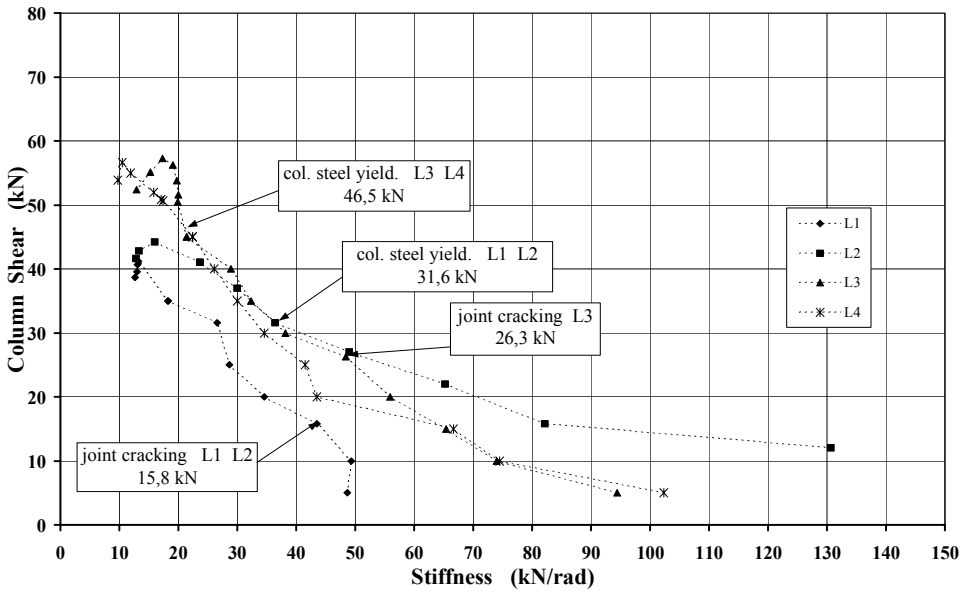

Figure 5. Column Shear vs. Secant Stiffness for Type L Connections

Total Energy: Type H Connections

The comparison is performed by using the control specimen as a reference (Figure 7). Connection H2 generally dissipates less than H1; in particular, before joint H2 starts cracking (column shear equal to 21 kN) its dissipated energy is about 20% less than H1. After first cracking of the joint, H2 reduces that gap, even though there is still a clear difference equal to about 10% less

than H1. A similar trend is provided by H3 as compared to H1. Before first cracking of the joint occurs (column shear equal to 21 kN), H3 dissipates about 55% less than H1; the occurrence of joint cracking makes H3 more energy dissipating, but its values remain constantly 40% less than those of H1. Connection H4 shows always-lower dissipated energy than H1; the difference remains constant after joint H1 starts cracking (column shear of 15.8 kN) and equal to 60% on average.

The above remarks resulted by comparing total energies corresponding to the same column shear. However, significant insights could also be obtained by comparing total energies at similar story drift angle in order to check how different upgrade schemes influence the energy that the subassemblage is able to dissipate before reaching a given drift angle. For type H specimens, a similar comparison is proposed in Figure 9: total energies corresponding to drift angles of 0.5%, 0.75% and 1% are depicted. It appears that the specimen with NSM bars and wrapping on the columns (i.e., H3) has the best energy dissipation capacity. The addition of FRP reinforcement to the joint limits its deformability as confirmed by lower energy values provided by H4 as compared to H3, for equal story drift angles. The increase of total energy with the story drift angle appears more regular for connections H3 and H4, while a clear trend cannot be derived by observing values given by H1 and H2.

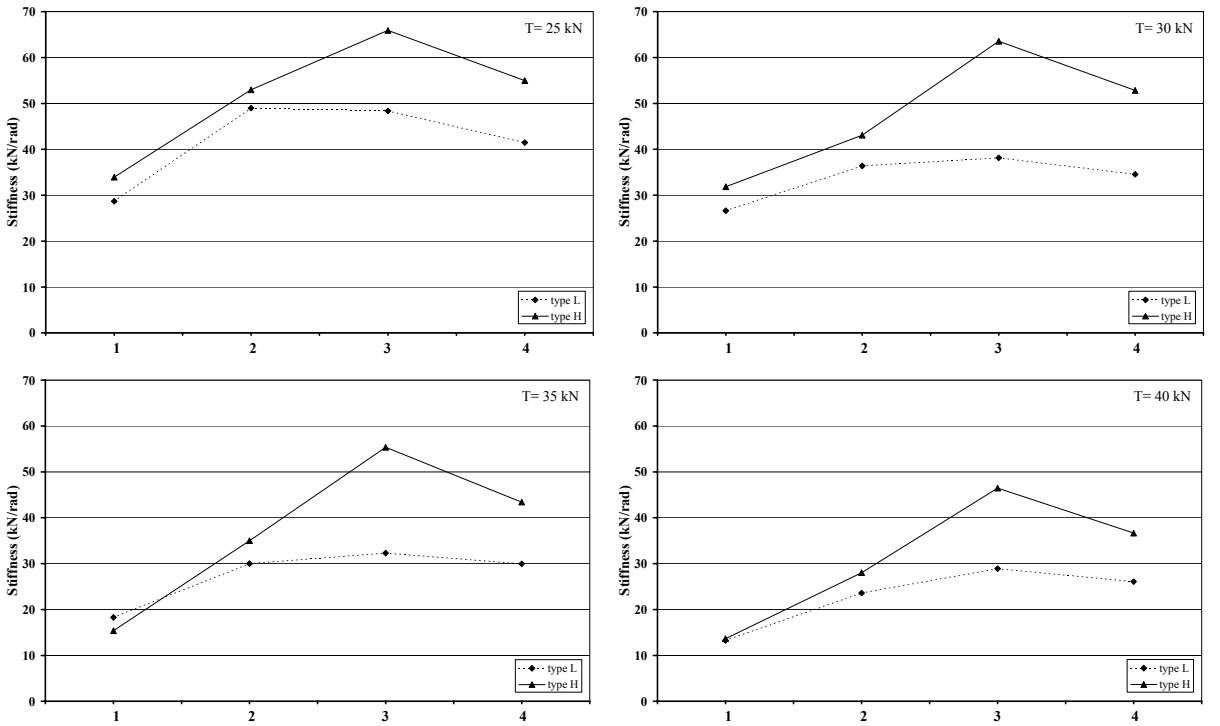

Figure 6. Comparison of Secant Stiffness between Type H and L Connections

Total Energy: Type L Connections

Total energies for type L subassemblaes are depicted in Figure 8. Specimens L1 and L2 reach joint cracking for the same column shear (15.8 kN). Before that, L2 dissipates about 44% more than L1; the first cracking of the joint reduces that gap between L1 and L2, even though L2 keeps dissipating about 15% more than L1. A different behavior is shown by L3 as compared to L1. Before L1 joint cracks, L3 dissipates about 30% more than L1. After joint cracking of connection L1, the difference decreases as the column shear increases. In the range 25-32 kN of column shear, there is the superposition of joint L3 cracking (26.3 kN) and steel yielding in L1 (31.6 kN); within that range, L1 and L3 become first similar and then the initial trend is inverted because L3 assumes energy values about 10% lower than L1. Before joint cracking of connection L1, the behavior of this

specimen is very similar to L4. As soon as cracking occurs in L1, L4 starts reducing its dissipation as compared to L1 with a constant difference of about 50%.

As previously discussed for type H specimens, interesting outcomes could be obtained by comparing the energy dissipation of type L subassemblages at fixed story drift angles. The analysis is showed in Figure 9 for drift angles of 0.5%, 1%, 1.5% and 2%. Also for this axial load ratio, the specimen with FRP bars and laminates on columns (i.e., L3) demonstrates the best energy dissipation capacity. Again, the addition of FRP reinforcement on the nodal zone influences the overall performance (i.e., L4) reducing its dissipation as compared to the case where no FRP reinforcement was applied to the joint. For any given drift angle, the lowest dissipation is achieved by the control connection (i.e., L1).

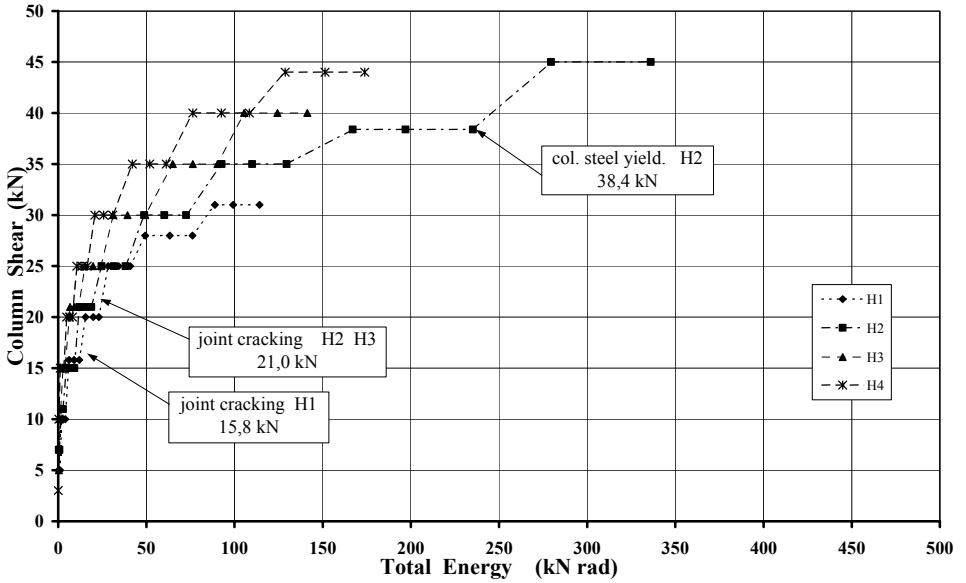

Figure 7. Column Shear vs. Total Energy: Type H connections

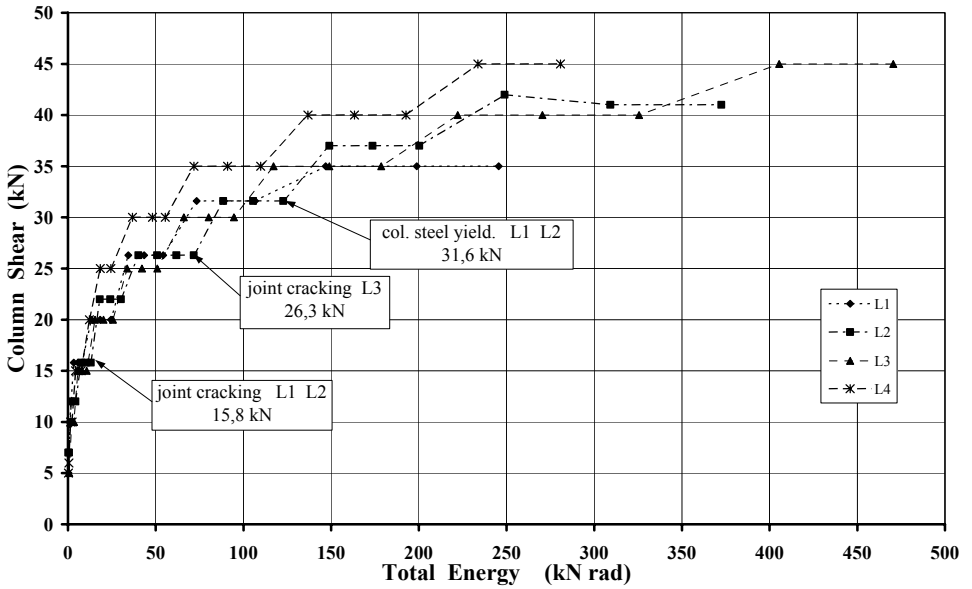

Figure 8. Column Shear vs. Total Energy: Type L Connections

Total Energy: Type H vs. Type L Connections

The different axial load ratio between type H (i.e., 0.2) and type L (i.e., 0.1) subassemblages is clearly reflected in the lower energy dissipation capacity that each type H specimen shows when compared to the similar type L connection. Specimen L1 provides energy values about 30% larger than H1. Connection L2 dissipates more than H2 with a difference ranging between 25% and 45%; after the steel yields in L2 (column shear of 31.6 kN), such gap becomes almost constant and equal to about 52%. The difference is even higher for subassemblages L3 and H3: before joint cracking of both, L3 dissipates up to 110% more than H3; then, the gap decreases and becomes very close to 90%. The energy dissipated by L4 is about 50% more than H4 up to a column shear of 30 kN; after that value, the difference increases and reaches values around 75%.

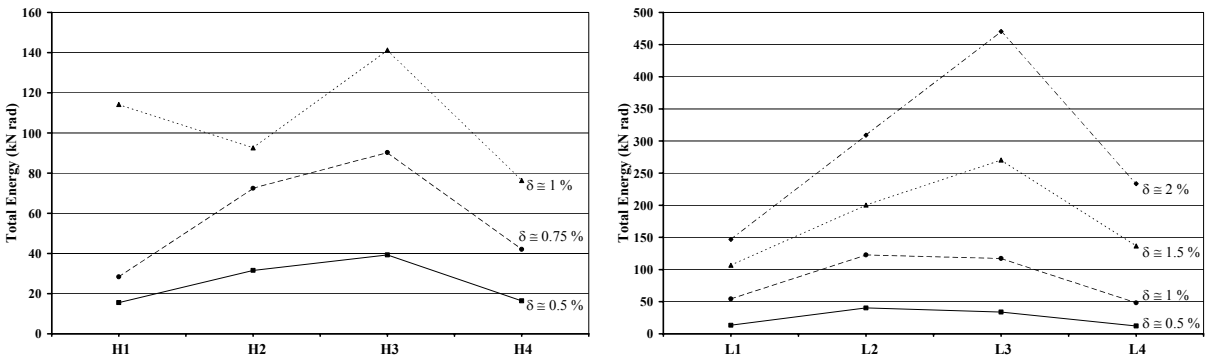

Figure 9. Total Energy at fixed Story Drift Angle for Type H and L Connections

Normalized Energy

Along with the total energy, values of normalized energy were also computed as shown in Figure 10-b. Such parameter indicates how much the loop corresponding to the first load repetition covers the area described by the vertical and horizontal lines drawn from the maximum points of the loop. Figures 11 and 12 show trends of such normalized energy for each series of tested specimens. It can be observed that the values of the normalized energy are generally larger for type L connections than for type H; this means that the shape of loops given by type L subassemblages tends to fit the rectangular area better than for type H. Within series H, connection H4 has the lowest normalized energy, followed by H3. After first cracking of joint H1, this connection behaves very similarly to H2; once H2 cracks, its shapes become larger than specimen H1. The yielding of column steel results in a drop of the normalized energy of H2 from 0.29 to 0.24. Similar remarks can be done for type L specimens. Again, connection L4 shows the lowest normalized energy. For the other three connections, L2 has larger loops than L1 and L3 until the latter experiences joint cracking. From that stage, L3 starts having the largest loops and L2 becomes intermediate between L1 and L3. Such order continues even after steel yielding in subassemblages L1 and L2.

Conclusions

The cyclic behavior of tested RC interior subassemblages has been assessed in terms of ductility (story drift angle), stiffness and dissipated energy. This analysis has underlined that:

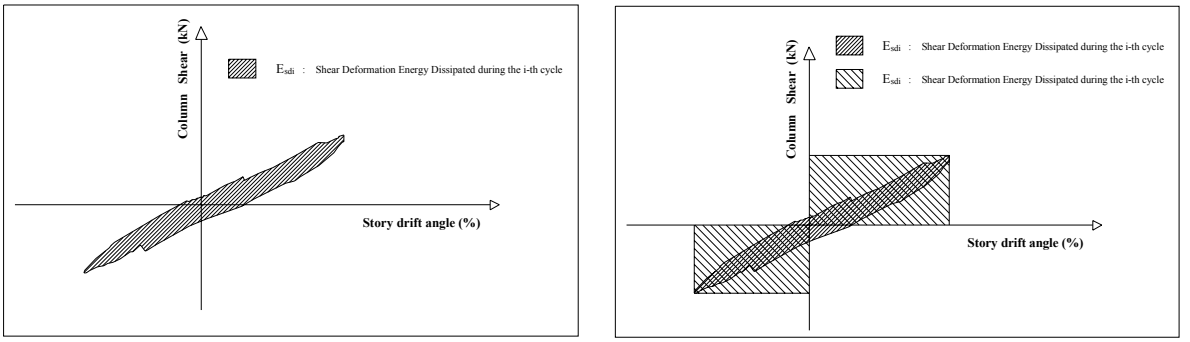

(a) (b)

Figure 10. Energy and Normalized Energy at the i-th Load Repetition

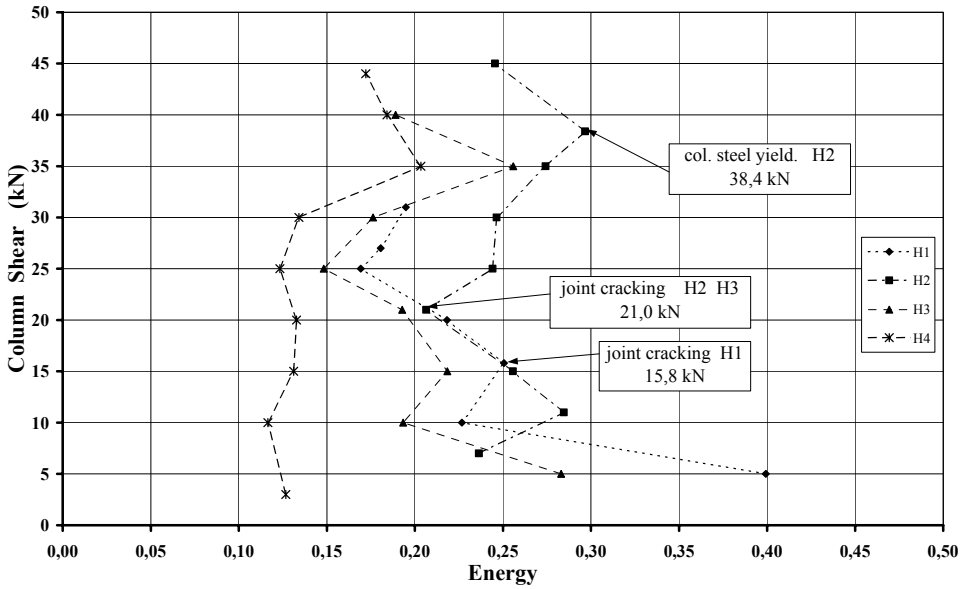

Figure 11. Column Shear vs. Normalized Energy at 1st Load Repetition: Type H Connections

- the influence of different upgrade schemes on the ultimate ductility of the subassemblage can vary depending on axial load ratio and concrete strength. This points out that a comprehensive assessment of the structural and material properties represents a preliminary step towards the selection of the most effective strengthening solution.
- between connections with the same axial load ratio, the influence of the FRP upgrade on the stiffness changes as critical stages (first cracking of the joint or steel yielding in the columns) are reached. Regardless of the upgrade scheme, a lower stiffness always corresponds to connections subjected to lower axial load.
- the analysis of total dissipated energy underlines that the lowest dissipation corresponds to connections with FRP reinforcement on both columns and joint. The same outcome was not found in terms of stiffness, even though it could be expected as the strengthening of the joint reduces its deformability. The authors believe that this is probably due to local effects causing specimens with NSM bars and laminates on columns to exhibit the highest stiffness.

The proposed analysis points out that increasing the strength could result in reducing the ductility or the energy dissipation capacity of the sub-system. For example, the strengthening of the joint (connections H4 and L4) boosts both strength and ductility (story drift angle), while it determines a very brittle post-peak behavior and reduces the dissipating capacity of the

subassemblage. Such outcomes could provide very significant insights for optimizing the selection and the configuration of the FRP strengthening within a performance-based approach.

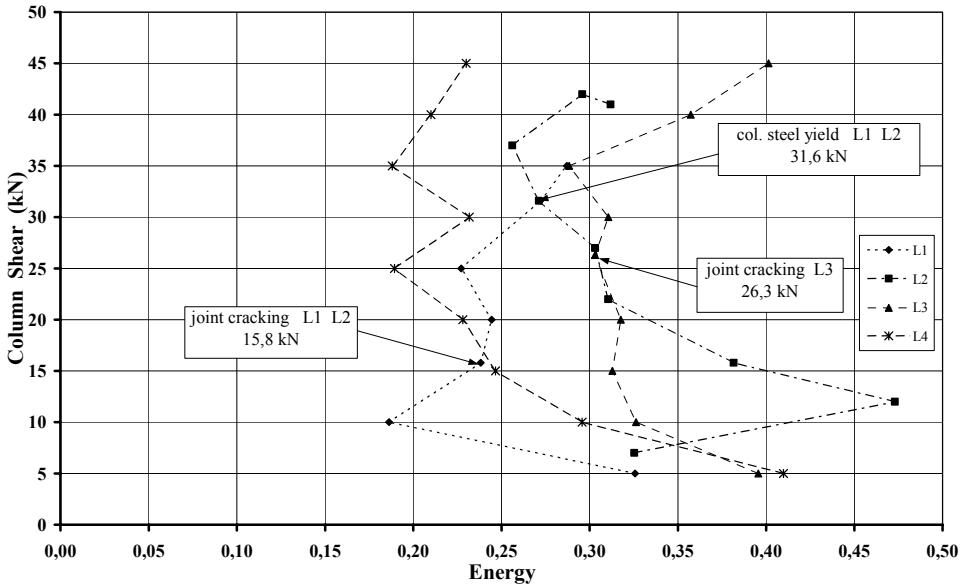

Figure 12. Column Shear vs. Normalized Energy at 1st Load Repetition: Type L Connections

Acknowledgements

The authors wish to acknowledge the support of the NSF Industry/University Cooperative Research Center – Repair of Buildings and Bridges with Composites at UMR.

References

1. ATC40 (1996), "Seismic Evaluation and Retrofit of Concrete Buildings", *California Seismic Safety Commission, Report SSC 96-01*.
2. FEMA 356 (2000*),* "Prestandard and Commentary for the Seismic Rehabilitation of Buildings"*, Prepared by American Society of Civil Engineers for Federal Emergency Management Agency,* Washington, D.C., US.
3. Ghobarah, Ahmed (2001), "Performance-based Design in Earthquake Engineering: State of Development", *Engineering Structures*, 23(8), pp. 878-884.
4. Higazy, El M. and Elnashai, Amr S. (1997), "Energy-based Technique for Seismic Performance Assessment of Interior Beam-Column Joints", *Journal of Earthquake Engineering*, 1(4), pp. 675-692.
5. Kupfer, Helmut B. and Gerstle, Kurt H. (1973), "Behavior of Concrete under Biaxial Stresses", *Journal of the Engineering Mechanics Division*, 99(4), pp.853-866.
6. Manfredi, Gaetano (2001), "Evaluation of Seismic Energy Demand", *Earthquake Engineering and Structural Dynamics*, 30(4), pp. 485-499.
7. Paulay, Thomas and Priestley, M. J. Nigel (1992) "Seismic Design of Reinforced Concrete and Masonry Buildings"*,* John Wiley & Sons, Inc., New York.

8. Priestley, M. J. Nigel (1997), "Displacement-Based Seismic Assessment of Reinforced Concrete Buildings", *Journal of Earthquake Engineering*, 1(1), pp. 157-192.
9. Priestley, M.J. Nigel, Seible, Frieder and Calvi, Gian M. (1996), "Seismic Design and Retrofit of Bridges", John Wiley & Sons, Inc., New York.
10. Prota, Andrea; Manfredi, Gaetano; Nanni, Antonio and Cosenza, Edoardo (2002a), "Selective Seismic Strengthening of RC Frames with Composites", *Proceedings of the Seventh US National Conference on Earthquake Engineering,* July 21-25, 2002, Boston, Massachusetts, USA (accepted).
11. Prota, Andrea; Manfredi, Gaetano; Nanni, Antonio and Cosenza, Edoardo (2002b), "Capacity Assessment of GLD RC Frames Strengthened with FRP", *Proceedings of the Twelfth European Conference on Earthquake Engineering*, September 9-13, 2002, London, UK (accepted).
12. Realfonzo, Roberto; Prota, Andrea; Manfredi, Gaetano and Pecce, Marisa (2002), "Flexural Strength of FRP-Confined RC Columns", *Proceedings of the First fib Congress,* October 13-19, 2002, Osaka, Japan (submitted).
13. Uang, Chia-Ming and Bertero, V.V. (1990), "Evaluation of Seismic Energy in Structures", *Earthquake Engineering and Structural Dynamics*, 19, pp. 77-90.